Icarus 211 (2011) 1274–1283

Contents lists available at ScienceDirect

Icarus

journal homepage: www.elsevier.com/locate/icarus

Central pit craters on Ganymede

Nathalia Alzate [a], Nadine G. Barlow [b,*]

[a] Department of Physics, Auburn University, Auburn, AL 36849-5311, United States
[b] Department of Physics and Astronomy, Northern Arizona University, NAU Box 6010, Flagstaff, AZ 86011-6010, United States

ARTICLE INFO

Article history:
Received 21 December 2009
Revised 14 October 2010
Accepted 15 October 2010
Available online 29 October 2010

Keywords:
Ganymede
Cratering
Mars, Surface
Ices

ABSTRACT

Central pit craters are common on Mars, Ganymede and Callisto, and thus are generally believed to require target volatiles in their formation. The purpose of this study is to identify the environmental conditions under which central pit craters form on Ganymede. We have conducted a study of 471 central pit craters with diameters between 5 and 150 km on Ganymede and compared the results to 1604 central pit craters on Mars (diameter range 5–160 km). Both floor and summit pits occur on Mars whereas floor pits dominate on Ganymede. Central peak craters are found in similar locations and diameter ranges as central pit craters on Mars and overlap in location and at diameters <60 km on Ganymede. Central pit craters show no regional variations on either Ganymede or Mars and are not concentrated on specific geologic units. Central pit craters show a range of preservation states, indicating that conditions favoring central pit formation have existed since crater-retaining surfaces have existed on Ganymede and Mars. Central pit craters on Ganymede are generally about three times larger than those on Mars, probably due to gravity scaling although target characteristics and resolution also may play a role. Central pits tend to be larger relative to their parent crater on Ganymede than on Mars, probably because of Ganymede's purer ice crust. A transition to different characteristics occurs in Ganymede's icy crust at depths of 4–7 km based on the larger pit-to-crater-diameter relationship for craters in the 70–130-km-diameter range and lack of central peaks in craters larger than 60-km-diameter. We use our results to constrain the proposed formation models for central pits on these two bodies. Our results are most consistent with the melt-drainage model for central pit formation.

1. Introduction

Central pit craters, which display a central depression either directly on the crater floor or atop a central uplift or peak, are common on Mars, Ganymede, and Callisto, all of which display volatile-rich crusts. Only a very small number of possible central pit craters have been reported for the Moon (Allen, 1975; Schultz, 1976), and the depressions seen on the floors of some impact craters on Mercury are different in morphology and location than the central pits on Mars, Ganymede, and Callisto, indicating that Mercury pits form by a different mechanism (likely subsurface magma withdrawal and floor collapse) (Gillis-Davis et al., 2009). The greater frequency of central pit craters on Mars, Ganymede, and Callisto suggest that target volatiles are necessary for the formation of impact crater central pits.

This study focuses on central pit craters on Ganymede, which has an icy crust of nearly pure H_2O (Pilcher et al., 1972; McCord et al., 1998, 2001). Ganymede central pit craters were first observed in Voyager imagery in 1979 (Fig. 1), which suggested that most craters on Ganymede between approximately 30- and 180-km-diameter displayed a central pit (Passey and Shoemaker, 1982; Schenk, 1993). Craters containing central peaks were reported at smaller crater diameters, transitioning to central pit craters at about 30-km-diameter. Central pits in turn transition into anomalous dome craters around 60-km-diameter, which display an uplifted central dome surrounded by a moat (Schenk, 1993).

This analysis is the first to utilize both Galileo and Voyager imagery to study central pit craters on Ganymede. The best Voyager image resolution of Ganymede was about 0.5 km/pixel and the Galileo mission improved these resolutions to better than 50 m/pixel in selected areas. However, neither mission imaged the entire moon at these high resolutions. Slightly more than 70% of Ganymede was imaged at 2 km/pixel resolution or better but less than 15% is imaged at better than 1 km/pixel resolution. Hence the image resolution varies considerably across the moon, making global analyses difficult. This study uses the best image data acquired by both Voyager and Galileo to investigate the characteristics of central pit craters on Ganymede.

The distribution and sizes of central pit craters across Ganymede can help to constrain the environmental conditions under which central pit craters form. Several formation models have been proposed for central pits in impact craters, all invoking

* Corresponding author.
E-mail addresses: NZA0010@auburn.edu (N. Alzate), Nadine.Barlow@nau.edu (N.G. Barlow).

0019-1035/$ - see front matter © 2010 Elsevier Inc. All rights reserved.
doi:10.1016/j.icarus.2010.10.015

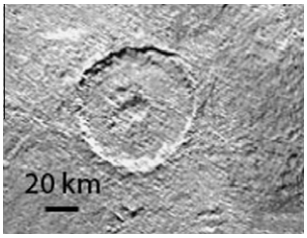

Fig. 1. Seventy-three-km-diameter Isis crater, located at 67.3°S 158.9°E, is an example of a central pit crater on Ganymede.

the volatile-rich nature of the crust. Wood et al. (1978) proposed that central pits were a result of gas release due to heating and vaporization of ice during crater formation. While numerical simulations show that impacts into ice-rich targets produce temperatures higher than the ice vaporization temperature near the center of the transient cavity (e.g., Pierazzo et al., 2005), most of the vapor produced during the excavation stage will escape prior to the period when the pit morphology can be retained (during the modification stage).

Another model for central pit formation invokes collapse of a central peak in weak target materials (Passey and Shoemaker, 1982). According to this model, the weight of the central peak exceeds the strength of the underlying material, causing the entire peak to collapse from its base and producing a pit. A related model explains pits on top of central peaks by partial collapse of brecciated material within the core of the central peak, a process enhanced by inclusion of ice in the peak material (Croft, 1981).

A third model proposes that layered target material preferentially produces central pits. Greeley et al. (1982) performed a series of gas-gun experiments simulating impacts into targets consisting of compositionally diverse layers. These experiments produced central pits when high velocity projectiles impacted into targets with varying combinations of ice, water, clay, and sand layers.

Central pit craters larger than ~60-km-diameter on Ganymede and Callisto display a dome in the center of the pit (Croft, 1983; Schenk, 1993). Schenk (Schenk, 1993; Schenk et al., 2004) proposes that the central dome results either from rapid uplift of deep material during crater formation or post-impact diapirism. In this model, "normal" pits (i.e., those without domes) are simply a precursor stage where the uplift or diapir does not occur or does not reach the surface. This model, however, only applies to central pit craters on Ganymede and Callisto; central pits on Mars would have to form by a different mechanism.

A final model for the formation of central pit craters is the melt-drainage model, which proposes that liquid is produced near the impact point during crater formation into ice-rich targets. This melt can form a transient liquid lake on the floor of the crater which subsequently drains into subfloor fractures during the post-impact period, leaving behind a central pit (Croft, 1981; Bray, 2009; Senft and Stewart, 2009; Elder et al., 2010; Senft and Stewart, Modeling the morphologic diversity of impact craters on icy satellites, submitted to Icarus (henceforth, Senft and Stewart, submitted for publication)).

Numerical modeling suggests that target rheology, particularly thermal gradient, plays a significant role in the production of interior crater morphologies, including central peaks and pits (Bray et al., 2008; Bray, 2009; Senft and Stewart, 2009, submitted for publication). Laboratory studies of hypervelocity impacts into ice-rich targets also find that ice temperature, target strength and porosity, compositional variations, and impactor properties influence final crater morphometry (Lange and Ahrens, 1983, 1987; Grey and Burchell, 2003; Burchell et al., 2001, 2005). Laboratory experiments show that central pits grow smaller, shallower, and less defined as ice temperature decreases (Burchell et al., 2001, 2005; Grey and Burchell, 2003). However, the small craters produced in these laboratory experiments form within the strength regime of crater mechanics, unlike the Ganymede craters in this study for which gravity dictates the final crater morphology. Also, the pits in the experimental craters formed by different processes than those proposed for central pits on Mars, Ganymede, and Callisto. Thus, these laboratory experiments are not applicable to the crater sizes in this study.

We have compiled a database of the distribution, sizes, and morphologic characteristics of central pit craters across Ganymede in order to test the different formation models against actual observations. This is the first study of central pit craters on Ganymede to incorporate both Galileo and Voyager imagery, and the first to compare the results with a new companion study of central pit craters on Mars. The comparison with martian central pit craters allows us to investigate how gravity and surface composition affect central pit characteristics on the two bodies. Comparisons of characteristics among Ganymede central pit craters as a function of crater diameter (and thus excavation depth) allow us to determine how crustal strength and thermal gradient influence the collapse process. The results therefore provide us with improved insights into the environmental factors favoring central pits and allow us to place constraints on the central pit formation models.

2. Methodology

We utilized data collected by the Galileo Solid State Imager (SSI) (Belton et al., 1992), which, with resolutions of ~50–200 m/pixel, allowed us to perform in-depth analysis to complement analyses conducted with the earlier Voyager Imaging Science Subsystem (ISS) data (Smith et al., 1977). The best images from both Galileo and Voyager were obtained from the Planetary Data System and used in this analysis to characterize central pit craters on Ganymede. We compiled a catalog of impact crater morphologic and morphometric information for all craters $\geqslant$5-km-diameter on Ganymede within the ±60° latitude zone. This catalog contains 5441 craters, of which 471 (8.65%) are classified as central pit craters. Each crater entry contains information on location, size, preservation state, geologic unit, and interior morphology. All measurements and comparison analyses were conducted using Geographic Information System (GIS) software and the US Geological Survey GIS maps of Ganymede (webgis.wr.usgs.gov/pigwad/maps/ganymede.htm).

The morphologic appearance of each crater was used to determine its preservation state. Classification of preservation is difficult for Ganymede due to the varying sun angles of the images. Most regions are imaged only once at sun angles that can be very high or very low. High sun angles reduce contrast, which increase the difficulty in determining morphometric characteristics such as rim sharpness and apparent crater depth. We therefore rely more on identification of distinguishing morphologic features (interior and ejecta morphologies) in high sun images to determine preservation class. With these caveats in mind, we have classified Ganymede craters on a scale of 1–3, with 1 indicating a highly degraded crater and 3 corresponding to a very fresh crater. Craters in preservation class 1 tend to be shallow and rimless with no preserved ejecta blanket and heavily eroded interior structures (if any remain). Preservation class 2 craters display an intermediate level of degradation, often retaining some portion of their upraised rim and interior structures. Class 2 craters appear deeper than class 1 craters, but shallower than fresh (class 3) craters of comparable size. Ejecta blankets are missing or highly degraded for class 2 craters. Preservation class 3 craters are very fresh, displaying sharp upraised rims, clearly discernible ejecta blankets, obvious interior

structures, and depths close to those expected for fresh craters of similar size (Schenk, 1993). Preservation class is a proxy for crater age within a specific region, but because of variations in the types and intensities of degradational processes across the moon, craters of different preservational states in widely separated regions may be geologically contemporaneous.

We analyzed central pit distribution by geologic unit to determine if regional or latitudinal variations occur. We utilized the USGS 1:5,000,000-scale geologic maps for Ganymede to identify the geologic units and determine if central pit craters preferentially form on specific geologic units. The geologic maps were produced from Voyager data and hence areas imaged by Galileo but not Voyager did not have corresponding geologic maps. In these cases we assigned generalized geologic units (e.g., cratered terrain, grooved terrain, etc.) to the regions so we could compare with the mapped areas.

Pit and crater diameters were measured and the pit diameter (D_p) to crater diameter (D_c) ratios were computed. We investigated variations in D_p/D_c as a function of crater diameter, geologic unit, and latitude. Impact craters excavate to a depth which is proportional to the crater diameter, and thus knowledge of the diameter gives insights into how deeply the craters are excavating into the subsurface. Schenk (2002) identified three depth–diameter transitions for Ganymede, one associated with the transition from simple to complex crater morphology at about 2-km-diameter, a second around ~26-km-diameter where central pits and central domes dominate, and the third in the realm where anomalous dome craters prevail ($D \sim 150$ km). Schenk (2002) argued that the depth–diameter changes corresponding to the second and third transitions occur as craters excavate into subsurface layers containing weaker ice and liquid, respectively. Excavation depth is proportional to transient crater diameter (D_t) regardless of the final depth–diameter value. McKinnon and Schenk (1995) derived a relationship between final crater diameter (D) and D_t (both in km) for complex craters:

$$D = 1.176 D_t^{1.108} \quad (1)$$

The excavation depth (d) is related to the transient crater diameter by (Melosh, 1989)

$$d_{ex} = 0.1 D_t \quad (2)$$

We calculated the transient crater diameter for each observed central pit crater using Eq. (1) and used that result to determine the excavation depth using Eq. (2). Using these results, we investigated whether excavation depths showed any variations among different geologic units, latitudes, or as a function of crater preservational state. Variations in excavation depth with location or time could imply changes in subsurface structure, which have implications for some of the proposed central pit formation models.

3. Observations

Martian central pits are either floor pits (pit occurs directly on crater floor) or summit pits (pit occurs atop a central peak) (Fig. 2) and are classified based on whether the floor of the pit lies below (floor pit) or above (summit pit) the lowest elevation of the crater floor. Some martian floor pits display a raised rim while others are rimless. Although a few summit pits have been reported for Ganymede (e.g., Bray, 2009), this analysis finds no unequivocal examples of summit pits occurring on top of central peaks. Some Ganymede central pits display raised rims and have been classified as summit pits in previous studies, but the martian examples suggest that these could be rimmed floor pits (Fig. 2). Therefore all Ganymede central pit craters in this analysis are classified as floor pit craters. Some of these pits occur on up-arched ("updomed") crater floors caused by immediate or post-impact rebound resulting from relaxation of the ice-rich crust (Schenk, 1993; Dombard and McKinnon, 2000). A topographic study of martian floor pit craters shows no sign of updoming of those crater floors, indicating a much lower target ice concentration (Kagy and Barlow, 2008).

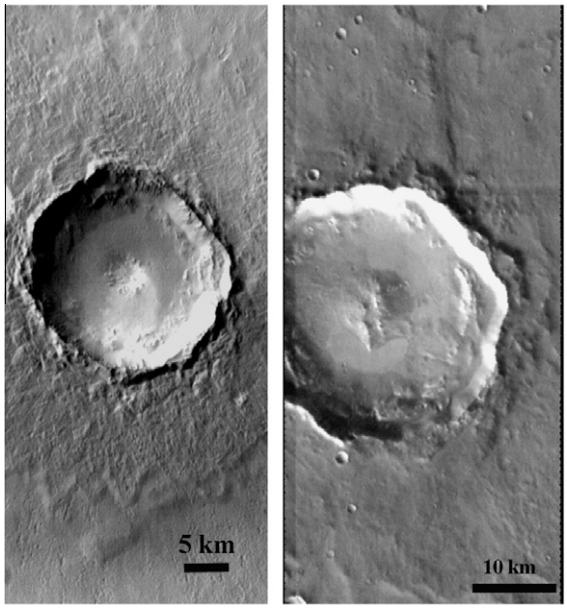

Fig. 2. Examples of martian floor pit and summit pit craters. (Left) This 24.8-km-diameter crater displays a 5.2-km-diameter floor pit. Crater is located at 0.77°N 356.06°E (THEMIS image I11284045). (Right) A 3.2-km-diameter summit pit tops the central peak of this 30.8-km-diameter crater centered at 0.45°N 296.91°E (THEMIS image I24502007).

3.1. Distribution of central pit craters

Central pit craters are common over all terrains on Ganymede. Fig. 3 shows the frequency of central pit craters on Ganymede as a function of latitude, normalized to the area (in km^2) covered within each latitude zone. Our study only included craters within the ±60° latitude zone in order to directly compare with the martian results (polar deposits affect central pit crater results at latitudes poleward of 60° on Mars). The data suggest a slightly higher concentration of central pit craters in the equatorial region than at higher latitudes, but the degrading resolution of the imagery at higher latitudes, particularly in the north, may explain this suggested trend.

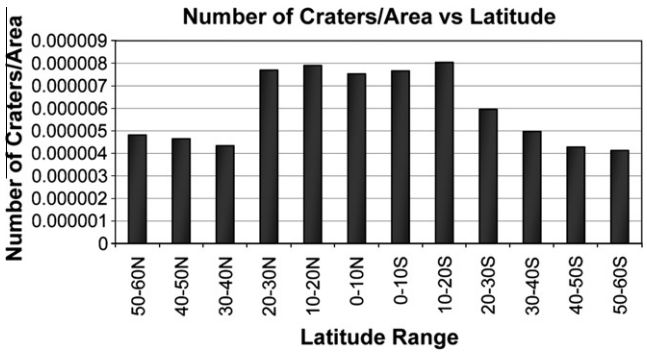

Fig. 3. Distribution of Ganymede central pit craters as a function of latitude. The number of craters in each 10° latitude zone is divided by the area (in km^2) of each latitude zone to adjust for the smaller areas at higher latitudes.

Earth-based spectroscopic studies suggested that as much as 90% of Ganymede's surface is water ice (Pilcher et al., 1972) with the remaining 10% composed of non-ice constituents, possibly including silicates (Pollack et al., 1978; Sill and Clark, 1982; Clark et al., 1986). Galileo Near-Infrared Mapping Spectrometer (NIMS) data reveal that the ice and non-ice components are heterogeneously distributed across Ganymede's surface, with H_2O ice concentrated at the poles and on the leading hemisphere (Pappalardo et al., 2004). Both crystalline and amorphous ices have been identified (Hansen and McCord, 2004). Non-ice compounds display a patchy distribution in the equatorial and mid-latitudes and show little mixing with the H_2O ice component (McCord et al., 2001). NIMS analysis suggests that the non-ice components include hydrated and hydroxylated minerals, O_2, O_3, CO_2 (with the low albedo units showing higher CO_2 concentrations (Hibbitts et al., 2003), SO_2, C≡N (probably as HCN), and CH (Spencer et al., 1995; Noll et al., 1996; McCord et al., 1998, 2001; Hansen and McCord, 2004). Albedo variations across Ganymede are generally attributed to the presence of a thin silicate-rich lag deposit in the low albedo regions, produced by processes such as sublimation and mass wasting (Proctor et al., 1998, 2000). Crater density analyses indicate that low albedo regions have an estimated age of ~4 Ga whereas higher albedo materials have ages of ~2 Ga or younger (Strom et al., 1981; Murchie et al., 1989; Zahnle et al., 1998, 2003; Neukum et al., 1998; Schenk et al., 2004). The number of central pit craters is approximately equal among terrains of different albedo. We find 222 central pit craters on high albedo units and 249 on dark units. Hence, neither the ice–silicate ratio nor the overall age of the terrain influences the formation of central pit craters.

Fig. 4 shows the distribution of central pit craters across Ganymede. Perusal of the image suggests that central pit formation is favored in the western (leading) hemisphere of the moon. However, the eastern (trailing) hemisphere of Ganymede is not covered by the higher resolution imagery and the apparent decrease in central pit crater frequency appears to be the result of lower-resolution imagery in this area. We conducted a comparison study of central pit crater identification using higher resolution versus lower-resolution imagery and found that central pit identification was reduced by approximately 67% when relying only on lower-resolution imagery. Alternately, the lower density of central pit craters in the trailing hemisphere may be due to the apex–antapex asymmetry in cratering, where bright terrain on the leading hemisphere displays a crater density four times higher than bright terrain on the trailing hemisphere (Zahnle et al., 2003). However, if Ganymede has only recently achieved its synchronous orbit, as proposed by Zahnle et al. (2003), the apex–antapex asymmetry should not be as prominent for the older low albedo material (which dominates the trailing hemisphere) or for the larger craters in which most of the central pits are observed. This analysis also finds that the number of central pit craters on the leading hemisphere is greater than a factor of four compared to the trailing hemisphere.

3.2. Sizes of central pit craters

The most complete study of central pit craters on Ganymede prior to the current analysis was conducted by Schenk (1993) who identified 91 central pit craters using Voyager imagery. Schenk's study found that central pits occurred in craters ranging from approximately 35 to 175 km in diameter whereas central peaks dominated in smaller craters. That study found that domes occurred inside the pits for craters ⩾60-km-diameter and might occur in smaller craters but were not resolvable at Voyager resolutions.

The current study has increased the number and expanded the size range of central pit craters on Ganymede, with 471 central pit craters ranging in size from 5 to ~150 km in diameter (Fig. 5). We did not distinguish between pits with and without central domes since we agree with Schenk (1993) that most of the larger craters have domes inside the pits. Our study shows both central pit craters and central peak craters are present in the same regions on Ganymede (Fig. 6). This study includes 1256 central peak craters in the 5–60-km-diameter range. Thus central peaks overlap the diameter range of non-domed central pit craters. However, the frequency of central peak craters reaches its maximum at diameters less than 15 km compared to the frequency peak of 30–35-km-diameter for central pit craters (Fig. 5).

Pit diameter (D_p) relative to the diameter of host crater (D_c) may provide insights into the target characteristics at the time of central pit crater formation. Previous studies reported that D_p increases linearly with D_c up to ~70 km, but increases much faster in larger craters (Schenk, 1993; Bray, 2009). The larger sample size of this study confirms that trend. Fig. 7 shows that D_p/D_c for central pit craters on Ganymede ranges from 0.11 to 0.38, with a median of 0.19. Central pit craters <70 km in diameter display a linear relationship between pit and crater diameter, but craters between about 70- and 130-km-diameter display a different trend, with pits being progressively larger relative to the parent crater (Fig. 8). The two largest craters in this analysis, however, display anomalously

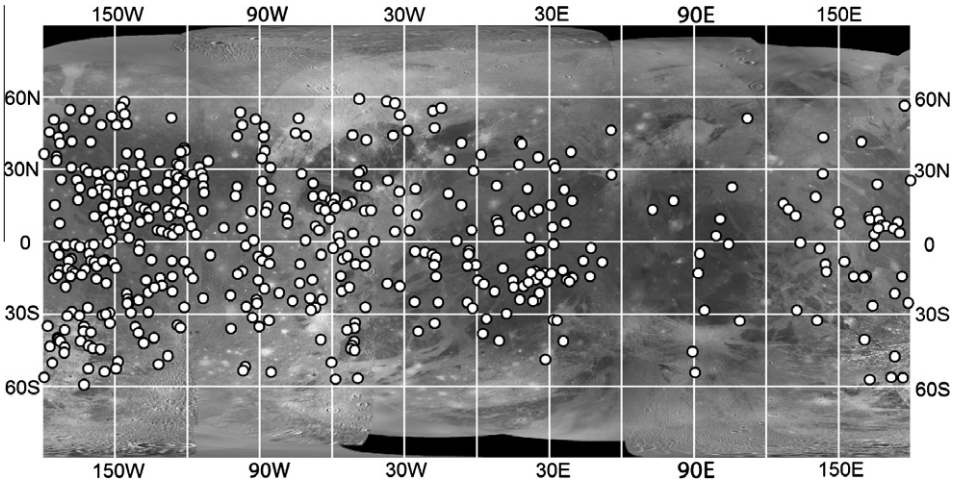

Fig. 4. Central pit crater distribution across Ganymede. The decrease in central pit crater frequency in the eastern (trailing) hemisphere likely results from lower-resolution imagery in this area.

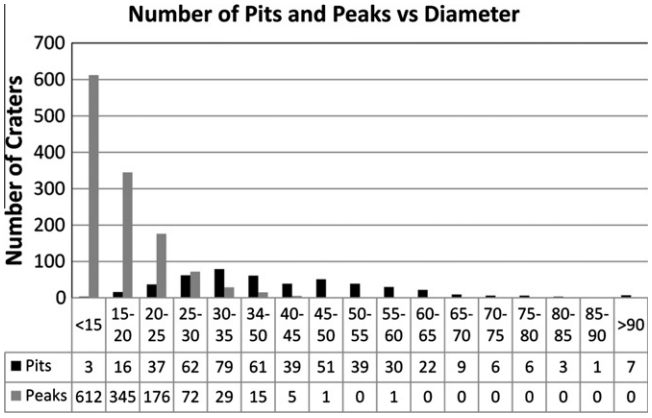

	<15	15-20	20-25	25-30	30-35	34-50	40-45	45-50	50-55	55-60	60-65	65-70	70-75	75-80	80-85	85-90	>90
Pits	3	16	37	62	79	61	39	51	39	30	22	9	6	6	3	1	7
Peaks	612	345	176	72	29	15	5	1	0	1	0	0	0	0	0	0	0

Fig. 5. Number of central pit and central peak craters as a function of diameter range (in km). Central pit craters on Ganymede range in diameter from 5 km to ~150 km. Central peak craters primarily occur in the 5–40-km-diameter range. Central pit and central peak craters overlap in the 15–40-km-diameter range. The number of craters with pits or peaks in each diameter range is shown in the table at the bottom of the graph.

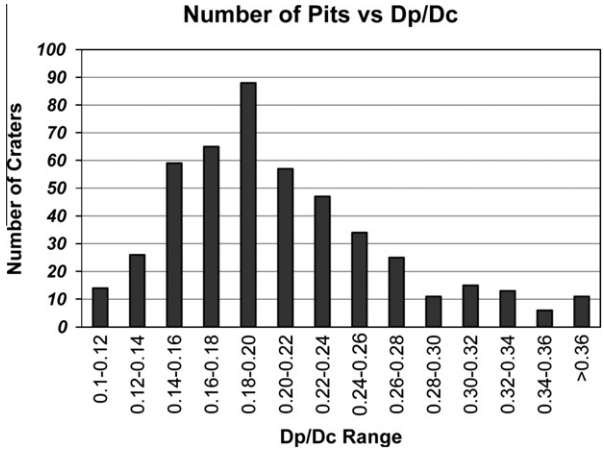

Fig. 7. Comparison of pit diameter (D_p) – crater diameter (D_c) ratios for central pits on Ganymede. The median value of D_p/D_c is 0.19.

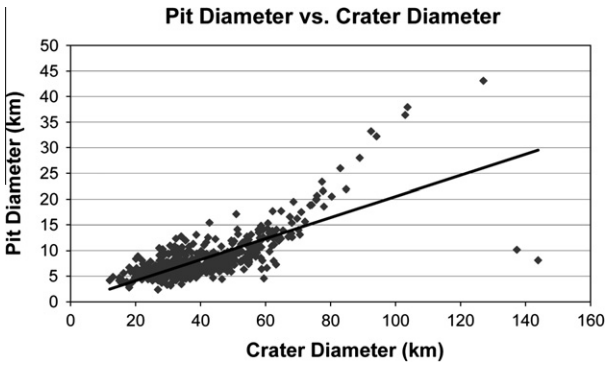

Fig. 8. Pit diameter versus crater diameter. Data follow a linear trend up to a crater diameter of about 70 km, then pits become much larger relative to their crater until the crater diameter reaches about 120 km. This trend suggests a change in subsurface properties at about 4 km depth.

small pits. These observations suggest that subsurface structure influences pit size. Using Eqs. (1) and (2), we find that craters following the linear trend excavated to less than 4 km depth whereas those in the 70–130-km-diameter range excavated to depths between 4 and 7 km. The larger pit diameters for the 70–130-km-diameter craters imply that the surface material is weaker in this depth range (Schenk, 2002), perhaps due to a change in the thermal gradient. Alternately, we may be seeing the effects of an ice phase transition, although the pressures at these depths are insufficient for phase transitions unassociated with shock from the impact itself. A weak zone around 4 km depth also is suggested by the lack of central peaks in craters >60-km-diameter. This could be related to the onset of pits with domes, which occur in craters >60-km-diameter (Schenk, 1993; Schenk et al., 2004)—the weaker zone may enhance the proposed post-impact diapirism mechanism. No variation of this trend is seen as a function of crater preservation class, and hence the conditions giving rise to this change in pit diameter are not indicative of temporal changes in interior structure. The much smaller pit diameters for craters >130-km-diameter suggest additional physical processes occur at depths greater than ~7 km, but the exact nature of these processes (increasing strength, changes in thermal gradient, changes in collapse processes, etc.) cannot be constrained simply on the basis of two data points.

3.3. Preservation states, geologic units, and excavation depths

The amount of degradation suffered by each crater is characterized through our three-point preservation class system, where class 1 craters are highly degraded and class 3 craters are extremely fresh. Of the 471 central pit craters in this analysis, 38% are class 1, 56% are class 2, and 6% are class 3. The presence of central

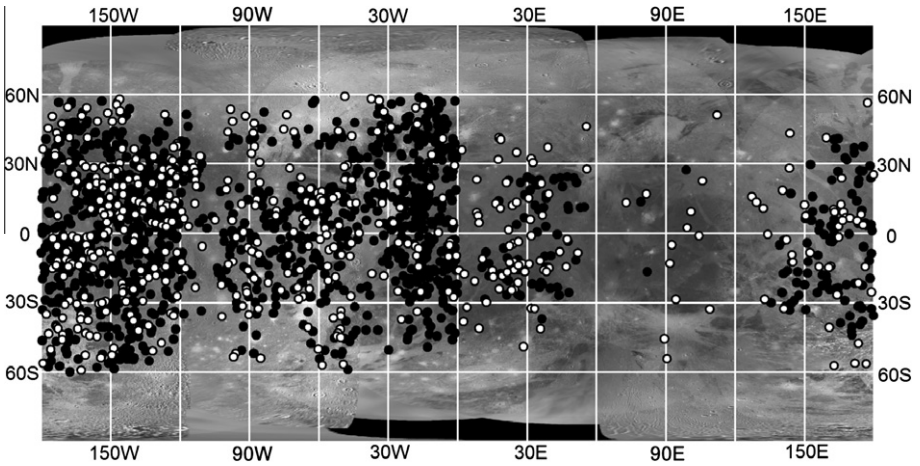

Fig. 6. Central pit (white) and central peak (black) crater distribution across Ganymede. Central peak craters occur in the same regions as central pit craters.

Table 1
Numbers of central pits on geologic units.

Geologic unit	Total # of craters	# Central pit craters	% Central pit craters
Dark			
Undivided (d)	1142	104	9
Cratered (dc)	1630	74	5
Furrowed (df)	317	58	18
Hummocky (dh)	7	1	14
Lineated (dl)	26	7	27
Reticulate (dr)	4	2	50
Smooth (ds)	201	10	5
Vermicular (dv)	180	5	3
Light			
Undivided (l)	180	30	17
Grooved (lg)	784	158	20
Smooth (ls)	81	20	25
Transitional (lt)	22	2	9

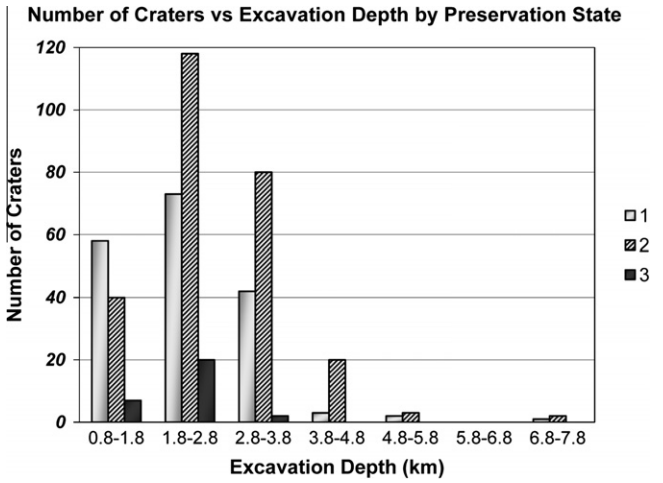

Fig. 9. Excavation depth of central pit craters as a function of crater preservation state. Crater preservation ranges from class 1 (very degraded) to 3 (very fresh). Most central pit craters excavate to depths between 1 and 4 km regardless of preservation state. There is no trend toward shallower or deeper excavation depths as a function of crater age.

pit craters in all three preservation classes indicates that conditions necessary for central pit formation have existed over the entire crater-retaining surface history of Ganymede.

We investigated central pit distribution as a function of geologic unit to determine whether central pits preferentially form on particular terrains. Table 1 summarizes the results of the geologic unit analysis. The only particularly high concentration of central pit craters occurs on dark reticulate (dr) terrain where 50% of the craters are central pits, but this unit has only four craters total so the results are not statistically significant. Central pits constitute 20% or less of all craters on all of the remaining geologic units except for the dark lineated (dl; 27%) and light smooth (ds; 25%) units. Overall we see no strong preference for the occurrence of central pit craters on any specific geologic unit. Crater depth analysis is useful in determining the influence of the subsurface environment on crater formation and morphology. We calculated the transient crater diameter from Eq. (1) and used these results in Eq. (2) to obtain excavation depth of all 471 central pit craters. Fig. 9 shows the frequency of central pit craters by preservation class as a function of excavation depth. Excavation depth ranges from 0.8 to 8.0 km, but central pit craters in all three preservation classes reach frequency peaks in the 1.0–3.0 km depth region. This constancy in excavation depth with preservational state indicates that the subsurface conditions necessary for central pit formation have not varied in depth over the period that craters have been retained on Ganymede's surface.

Table 2 includes information about excavation depth of central pit craters on different geologic units. Most central pit craters excavate to depths between 1 and 4 km regardless of geologic unit. There is a slight trend for excavation depths to be lower on high albedo units than on the darker areas, which may be a reflection of higher thermal gradients associated with the lighter grooved units.

3.4. Comparison of Ganymede and Mars central pit craters

We compare our results for central pit craters on Ganymede with a companion study of central pit craters on Mars (Barlow, 2007, 2009, 2010) to determine how target composition and surface gravity might affect central pit characteristics. Differences in central pit characteristics between Ganymede and Mars which cannot be easily explained by these factors would suggest different formation mechanisms for central pits on the two bodies.

Martian central pits occur both directly on the crater floor (floor pits) and atop central peaks (summit pits). The study identified 912 floor pit craters and 692 summit pit craters across the surface of Mars using Mars Odyssey Thermal Emission Imaging System (THEMIS) visible (18 m/pixel resolution) and daytime infrared (100 m/pixel resolution) imagery. The survey of central pit craters in the northern hemisphere of Mars is complete but the study is still continuing for the southern hemisphere (Barlow, 2006, 2009). Nevertheless, sufficient numbers of central pit craters have now been identified on Mars to permit a comparison study with their counterparts on Ganymede.

The distribution of floor pit craters on Mars shows no significant difference from the distribution of summit pit craters as a function of latitude, longitude, or geologic unit on Mars (Fig. 10). Martian floor pit craters have diameters between 5 and 160 km whereas summit pit craters range in diameter from 5.5 km to 125 km, indicating that there is no diameter preference as a function of pit type (Fig. 11). Central pits are found in craters with a wide range of preservation (Barlow, 2006, 2009), indicating that the conditions favoring central pit formation have existed on Mars for most if not all of the planet's history.

Central pit craters on Ganymede display a number of similarities to their counterparts on Mars in spite of the difference in surface composition (mainly ice for Ganymede; rock–ice mixture for Mars), surface temperature, and surface gravity. Central pit craters on both bodies show no correlation with specific geologic units, nor are there any strong regional trends in their distributions (Barlow, 2009, 2010). The presence of central pit craters in various preservational states indicates that the conditions under which these craters form have existed throughout the geologic histories of both Ganymede and Mars.

However, some differences are observed among central pit craters on the two bodies. Floor pits dominate on Ganymede whereas both floor and summit pits occur on Mars. This is likely due to the stronger rock–ice martian crust being able to preserve a central peak even when a pit forms. Many central pits on Ganymede occur on updomed crater floors as a result of post-impact rebound of the ice-rich target material (Schenk, 1993; Dombard and McKinnon, 2000). Martian floor pit craters show no evidence of updomed floors (Kagy and Barlow, 2008), indicating an ice concentration much lower than that in Ganymede's crust. The concentration of ice in the upper few kilometers of the martian crust varies considerably across the planet. For the ±40° latitude zone where most central pit craters are found, ice concentrations estimated from layered ejecta deposits (Woronow, 1981; Oberbeck, 2009) and the rheological properties of the martian permafrost (Durham et al., 2009) typically range between 20% and 35%. These low ice concentrations are consistent with the lack of updomed floors

Table 2
Number of central pit craters with specific excavation depth as a function of geologic unit.

Excavation depth (km)	*d*	dc	df	dh	dl	dr	ds	dv	*l*	lg	ls	lt
0.8–1.8	54	14	20	1	1	1	0	3	0	9	1	0
1.8–2.8	50	13	24	0	6	1	10	2	9	23	14	0
2.8–3.8	0	17	1	0	0	0	0	0	11	17	5	2
3.8–4.8	0	23	13	0	0	0	0	0	10	109	0	0
4.8–5.8	0	5	0	0	0	0	0	0	0	0	0	0
5.8–6.8	0	0	0	0	0	0	0	0	0	0	0	0
6.8–7.8	0	3	0	0	0	0	0	0	0	0	0	0

See Table 1 for information about geologic unit nomenclature.

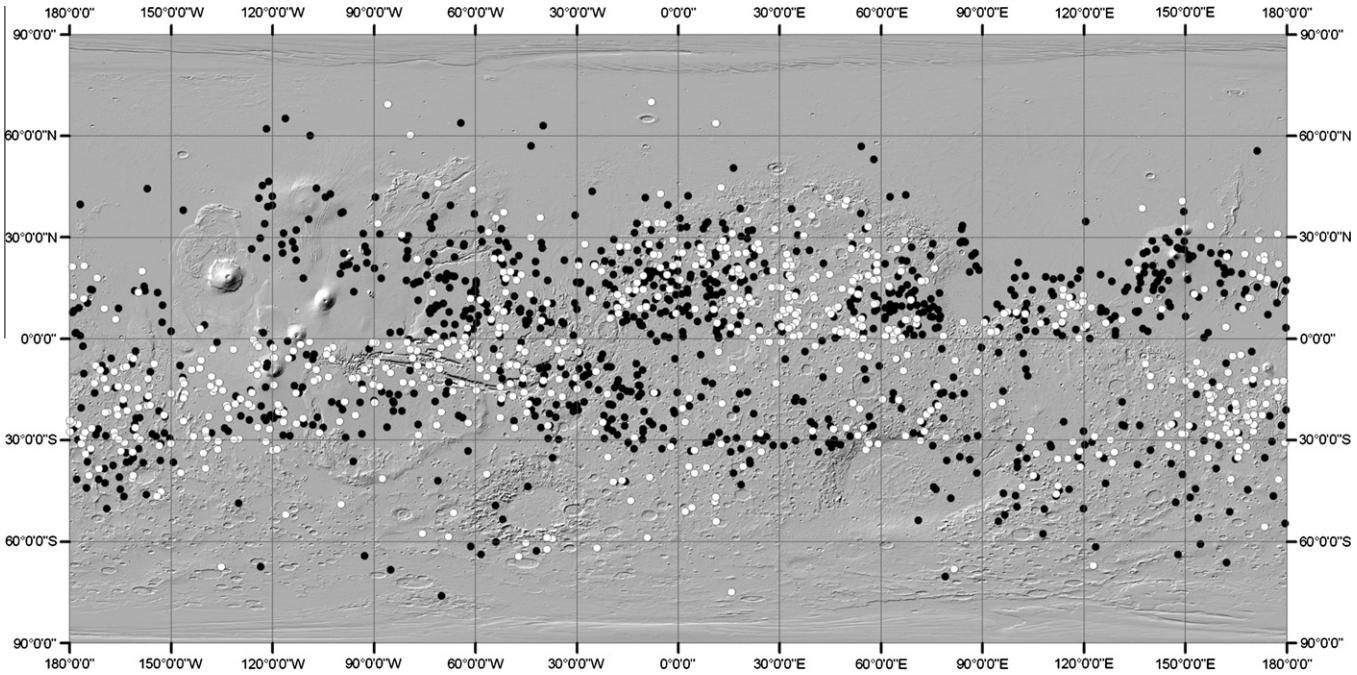

Fig. 10. Distribution of martian central pit craters. Both floor pits (black) and summit pits (white) are seen in the same regions and within the same topographic and geologic unit ranges.

and indicate that central pits can form in materials with a large range in ice concentration.

Central pit craters range from small (5 km, which is the lower diameter limit of both studies) to large (⩾100-km-diameter). Fig. 11 compares the occurrence of central pit craters on both bodies as a function of diameter range. The frequency peak for Ganymede central pit craters occurs near 35 km, about three times larger than the frequency peak for martian central pit craters (10–15-km-diameter range for floor pits and 10–20-km-diameter range for summit pits). The difference of ~3 for the frequency peaks between floor pit craters on Mars and central pit craters on Ganymede could be due to the difference in surface gravity. The acceleration of gravity for a body is given by

$$g = \frac{GM}{R^2} \tag{3}$$

where G is the gravitational constant (6.67×10^{-11} m^3 kg^{-1} s^{-2}), M is the mass of the body, and R is the body's radius. Surface gravity on Mars is 3.71 m s^{-2} whereas that on Ganymede is 1.42 m s^{-2}, a difference of 2.6. Crater transition diameter scales inversely with g, thus identical energy impacts will produce a larger crater on Ganymede than on Mars. Target density also influences the final crater size, and Ganymede's lower density crust would preferentially produce a larger crater for the same energy impact. However, the mechanical strength of Ganymede's icy crust is lower than the rock–ice crust of Mars which results in complex crater morphologies such as central peaks occurring at smaller crater diameters than their counterparts on the rocky Moon, which has similar surface gravity (1.63 m s^{-2}) to Ganymede (Schenk, 1991, 1993; Bray et al., 2008). Thus, the results indicating a higher frequency of pits in larger craters on Ganymede than on Mars are opposite of the trends seen for other complex crater morphologies on Ganymede versus the Moon. Either gravity dominates over mechanical strength in the formation of central pits or resolution is the culprit. Higher resolution images acquired by future orbiters should help resolve this conundrum.

Fig. 12 shows the frequency of central pit craters on both Ganymede and Mars as a function of D_p/D_c ratio ranges. Martian floor pits have D_p/D_c ranging from 0.02 to 0.48 (median of 0.16), whereas summit pits have D_p/D_c ranging from 0.03 to 0.29, with a median of 0.13. D_p/D_c values for Ganymede range from 0.11 to 0.38 with a median of 0.19. This indicates that Ganymede central pits tend to be larger relative to their parent crater than martian central pit craters, but only by a factor of 1.2 for comparable floor pits.

4. Discussion and implications for formation models

New image datasets combined with advances in theoretical modeling have expanded our understanding of central pit craters beyond the initial studies of the 1980s. This comparison study of

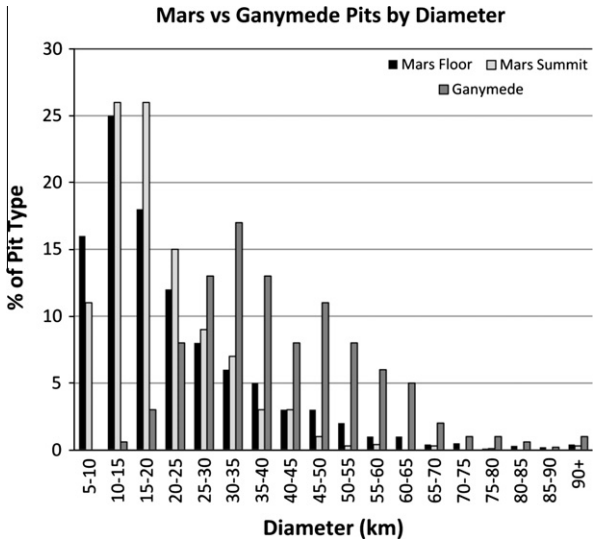

Fig. 11. Central pit craters on Mars and Ganymede as a function of diameter. Results are normalized to the total number of pit craters of the specific type (i.e., total number of Mars floor pit craters, total number of Mars summit pit craters, and total number of Ganymede pit craters). Floor pit craters on Mars exhibit a peak in their numbers in the 10–15-km-diameter range and summit pit craters peak in frequency between 10- and 20-km-diameter. Ganymede central pit craters peak in the 30–35-km-diameter range.

central pit craters on Ganymede and Mars leads to an improved understanding of common environmental conditions under which this unusual crater morphology forms. Observations from this study include the following:

- Central pit craters on Ganymede are dominantly floor pit craters whereas both floor and summit pit craters occur on Mars, probably because of the stronger rock–ice mixed crust on the latter.
- Some central pits occur on updomed floors on Ganymede due to immediate or post-impact rebound of the ice-rich crust (Schenk, 1993; Dombard and McKinnon, 2000). Lack of updomed floors in martian floor pit craters indicates that central pits can form in crusts with much lower concentrations of ice than those seen on Ganymede (Kagy and Barlow, 2008).
- No significant latitudinal or regional variations in central pit distribution are seen on either Ganymede or Mars. Central pits do not strongly favor a specific geologic unit on either body.

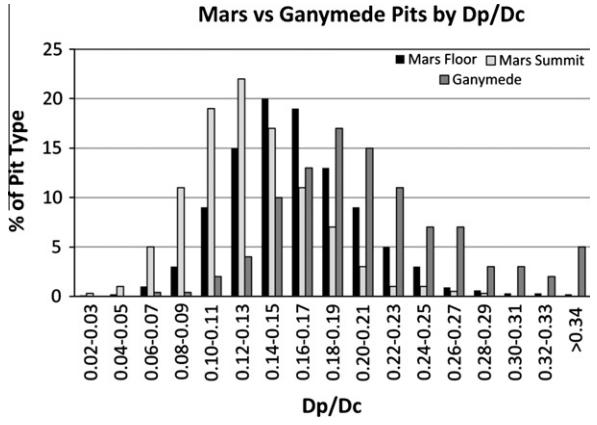

Fig. 12. Central pit craters on Mars and Ganymede as a function of D_p/D_c. Results are normalized to the total number of pit craters of the specific type (see caption for Fig. 11). Martian floor pit and summit pit craters have median D_p/D_c values of 0.16 and 0.13, respectively, whereas Ganymede pit craters have a median D_p/D_c of 0.19. This indicates that central pits on Ganymede tend to be larger relative to their parent crater than martian central pits. This difference is likely due to the purer ice crust on Ganymede.

- Central pit craters occur in a range of preservational states on both bodies, indicating that the conditions favoring central pit formation have existed for most if not all of the histories of both Ganymede and Mars (at least since crater-retaining surfaces have been present). Crater diameter, and thus excavation depth, does not vary as a function of preservational state.
- The frequency peak in central pit crater diameters is about three times larger on Ganymede than on Mars. This may be due to the 2.6 difference in gravity between the two bodies, or could be a resolution effect.
- Central pits on Ganymede tend to be larger relative to their parent crater than central pit craters on Mars. This may result from the purer ice content of the Ganymede crust enhancing the formation of central pits.
- We confirm the reports by Schenk (1993) and Bray (2009) that larger craters on Ganymede tend to have much larger pits than smaller craters. This is unlike Mars where the trend is linear at all sizes (slope of the linear segment is shallower on Mars than Ganymede, reflecting the smaller D_p/D_c). This suggests that pit size is influenced by excavation into weaker layers at depth in Ganymede.
- The diameter range of central peak craters (5–60 km) overlaps that of central pit craters (5–150 km) on Ganymede and both peaks and pits occur in similar regions of the moon. This overlap in diameter and location also is observed for peak and pit craters on Mars.

These observations of central pit craters on both Ganymede and Mars allow us to reevaluate the proposed formation mechanisms.

- *Central peak collapse model* (Passey and Shoemaker, 1982): Early observations reported that few central peaks were seen in craters in the diameter range where central pit craters were observed. This led to the proposal that central pits form by the collapse of a central peak forming in weak layered target material. Our observations reveal that central peak craters do occur in the same locations and diameter ranges as central pit craters on Ganymede, although the frequency of central peak craters is much reduced as the frequency of central pits increases. Martian central peak craters show strong overlap with central pit craters in both diameter and location (Barlow, 2010). Thus our observations of central pit versus central peak craters on both Ganymede and Mars, allow us to reject the model that central floor pits form by collapse of central peaks.
- *Uplift/diapirism model* (Schenk, 1993; Schenk et al., 2004): This model can explain the domes observed in craters >60-km-diameter on Ganymede, but it is unclear if central pits are a necessary precursor stage for these domes or if the conditions producing central pits simply enhance the uplift/diapirism necessary for dome formation in larger craters.
- *Layered target model* (Greeley et al., 1982): Greeley et al.'s laboratory simulations showed that layers of different compositions/densities can produce pit-like features, and there is some suggestion that martian floor pit craters preferentially form in volcanic regions where layering might be expected (Barlow, 2010). The experiments only considered layers of different compositions, not rheologies, and thus it is unclear whether they could apply to the uppermost crust of Ganymede. The other issue with this model is whether the laboratory results can be extrapolated to the formation of large impact craters in planetary settings.
- *Target ice vaporization model* (Wood et al., 1978): The target ice vaporization model is consistent with the lack of any regional or latitudinal variations in central pit concentrations on both Ganymede and Mars since ice is expected to occur globally within the near-surface crust of both bodies. Ice is expected to have

existed in Ganymede's crust since the surface became rigid enough to retain impact scars and has existed in the martian crust for most if not all of that planet's history, explaining the presence of central pits in craters of all preservational states. Observations of the pit and crater diameter ranges are consistent with the depths at which ice is expected to occur in both bodies and the observation of much larger pits for larger craters on Ganymede can be attributed to excavation into weaker subsurface ice layers at depth, something not expected for Mars which in fact does not show a deviation in the D_p versus D_c trend at larger crater diameters. However, the vaporization of target volatiles should occur during the excavation stage of crater formation and it is unclear how this vapor is trapped until the final crater cavity forms. So while our observations are consistent with this model, the mechanism for trapping the vapor during the excavation stage and then explosively releasing it after the final crater has formed has not been physically modeled.

- *Melt-drainage model* (Croft, 1981; Bray, 2009; Senft and Stewart, 2009, submitted for publication; Elder et al., 2010): The central pit observations outlined above for the ice vaporization model also support the melt-drainage model. Croft (1981) first proposed that summit pits could form by collapse of weak brecciated material in the core of central peaks and that the resulting pit would be more prominent if the peak material included liquid which would drain through the fractures within the brecciated interior of the peak. Recent numerical modeling of crater formation in ice using a multi-phase equation of state for H_2O reveals the formation of a hot plug in the bottom of the final crater cavity (Senft and Stewart, 2009, submitted for publication). This plug has a temperature high enough for melting to occur. At the end of crater formation, the ice is on the liquid phase boundary, allowing the melt to drain away into subsurface fractures and leaving behind a pit. Formation of the hot plug is sensitive to the impact energy, with lower energy impacts not creating the hot plug and very high energy impacts producing vapor rather than melt; neither of these situations will produce a central pit. This model can thus produce both floor and summit pits, explain the diameter range of central pit craters, and predicts plug-to-crater diameter ratios comparable to the observed pit-to-crater diameter ratios. The larger D_p/D_c ratios on Ganymede can be explained by higher amounts of melt being produced during impact into the purer ice crust. This model is consistent with all aspects of our observations of central pits on both Ganymede and Mars.

5. Conclusions

Central pit craters were first identified on Mars using Mariner 9 (Smith, 1976) and Viking (Hale and Head, 1981; Hale, 1982, 1983; Hodges, 1978; Hodges et al., 1980) data and on Ganymede using Voyager imagery (Smith et al., 1979; Passey and Shoemaker, 1982; Schenk, 1993). This is the first study to revisit Ganymede's central pit craters using higher resolution imagery from the Galileo spacecraft in combination with Voyager data, and the first study to compare the characteristics of central pit craters on Ganymede with a new study of their counterparts on Mars. We find several similarities between central pit craters on Ganymede and Mars, but also a number of differences which are consistent with expectations due to the different surface compositions (ice for Ganymede, mixed rock and ice for Mars), subsurface structures (weak subsurface layer at ~4 km depth on Ganymede), and surface gravity (which is 2.6 times stronger on Mars than on Ganymede). While different processes or a combination of processes cannot be completely ruled out based on our current data, we argue that the observed similarities among central pit craters on Mars and Ganymede (particularly for Ganymede central pit craters <60-km-diameter) are sufficient to suggest that these features form by a similar mechanism on both bodies. The results of this study do not support the central peak collapse model for central pit formation on both Ganymede and Mars, and there is no indication that central pit formation requires uplift/diaparism in the absence of central domes. While the results of this study can support the layered target and ice vaporization models, concerns remain about the applicability of these mechanisms for the formation of central pits on Ganymede and Mars. The melt-drainage model is most consistent with both our observations and the results of recent numerical simulations and can explain both floor and summit pit craters (Croft, 1981; Bray, 2009; Senft and Stewart, 2009, submitted for publication; Elder et al., 2010). The few issues remaining with this model, such as why craters with central pits can occur adjacent to non-pit craters of similar size and age and why not all martian layered ejecta craters (generally believed to form by impact into ice) display a central pit, may suggest an additional influence of impactor velocities (Senft and Stewart, submitted for publication).

Acknowledgments

The authors thank Sarah Stewart and an anonymous reviewer for their constructive comments which have greatly improved this manuscript. We also thank Ryan Godwin who helped compile the Ganymede crater catalog, Priyanjoli Mukherjee for assistance in the geologic unit analysis, and Jamie Housholder and Trent Hare for assistance with the GIS maps. This research was funded by NASA Outer Planets Research Program Award #NNG05GI16G.

References

Allen, C.C., 1975. Central peaks in lunar craters. Moon 12, 463–474.
Barlow, N.G., 2006. Impact craters in the northern hemisphere of Mars: Layered ejecta and central pit characteristics. Meteorit. Planet. Sci. 41, 1425–1436.
Barlow, N.G., 2007. Martian central pit craters: Characteristics, distribution, and comparison with central pit craters on Ganymede. Lunar Planet. Sci. XXXIX. Abstract 1242.
Barlow, N.G., 2009. Martian central pit craters: Summary of northern hemisphere results. Lunar Planet. Sci. XL. Abstract 1915.
Barlow, N.G., 2010. Central pit, central peak, and elliptical craters in the martian northern hemisphere: New results from the Revised Catalog of Large Martian Impact Craters. Lunar Planet. Sci. XLI. Abstract 1065.
Belton, M.J.S., Klaasen, K.P., Clary, M.C., Anderson, J.L., Anger, C.D., Carr, M.H., Chapman, C.R., Davies, M.E., Greeley, R., Anderson, D., 1992. The Galileo solid-state imaging experiment. Space Sci. Rev. 60, 413–455.
Bray, V.J., 2009. Impact Crater Formation on the Icy Galilean Satellites. PhD thesis, Imperial College London, 267pp.
Bray, V.J., Collins, G.S., Morgan, J.V., Schenk, P.M., 2008. The effect of target properties on crater morphology: Comparison of central peak craters on the Moon and Ganymede. Meteorit. Planet. Sci. 43, 1979–1992.
Burchell, M.J., Grey, I.D.S., Shrine, N.R.G., 2001. Laboratory investigations of hypervelocity impact cratering in ice. Adv. Space Res. 28, 1521–1526.
Burchell, M.J., Leliwa-Kipystyński, J., Arakawa, M., 2005. Cratering of icy targets by different impacts: Laboratory experiments and implications for cratering in the Solar System. Icarus 179, 274–288.
Clark, R.N., Fanale, F.P., Gaffey, M.J., 1986. Surface composition of natural satellites. In: Burns, J.A., Matthews, M.S. (Eds.), Satellites. Univ. of Arizona Press, Tucson, pp. 437–491.
Croft, S.M., 1981. On the origin of pit craters. Lunar Planet. Sci. XII, 196–198.
Croft, S.M., 1983. A proposed origin for palimpsests and anomalous pit craters on Ganymede and Callisto. Proc. Lunar Sci. Conf. 14, J. Geophys. Res. 88, B71–B89.
Dombard, A.J., McKinnon, W.B., 2000. Long-term retention of impact crater topography on Ganymede. Geophys. Res. Lett. 27, 3663–3666.
Durham, W.B., Pathare, A.V., Stern, L.A., Lenferink, H.J., 2009. Mobility of icy sand packs, with application to martian permafrost. Geophys. Res. Lett. 36, L23203. doi:10.1029/2009GL040392.
Elder, C.M., Bray, V.J., Melosh, H.J., 2010. Central pit formation in Ganymede craters via melt drainage. Lunar Planet. Sci. XLI. Abstract 2519.
Gillis-Davis, J.J., Blewett, D.T., Gaskill, R.W., Denevi, B.W., Robinson, M.S., Strom, R.G., Solomon, S.C., Sprague, A.L., 2009. Pit-floor craters on Mercury: Evidence of near-surface igneous activity. Earth Planet. Sci. Lett. 285, 243–250.
Greeley, R., Fink, J.H., Gault, D.E., Guest, J.E., 1982. Experimental simulation of impact cratering on icy satellites. In: Morrison, D. (Ed.), Satellites of Jupiter. Univ. of Arizona Press, Tucson, pp. 340–378.

Grey, I.D.S., Burchell, M.J., 2003. Hypervelocity impacts cratering on water ice–targets at temperatures ranging from 100 K to 253 K. J. Geophys. Res. 108 (E3), 5019. doi:10.1029/2002JE001899.
Hale, W.S., 1982. Central pits in martian craters: Occurrence by substrate, ejecta type, and rim diameter. Lunar Planet. Sci. XIII, 295–296.
Hale, W.S., 1983. Central structures in martian impact craters: Morphology, morphometry, and implications for subsurface volatile distribution. Lunar Planet. Sci. XIV, 273–274.
Hale, W.S., Head, J.W., 1981. Central structures in martian craters: Preliminary implications for subsurface volatile effects. In: Third International Colloquium on Mars. Lunar and Planetary Institute, p. 104.
Hansen, G.B., McCord, T.B., 2004. Amorphous and crystalline ice on the Galilean satellites: A balance between thermal and radiolytic processes. J. Geophys. Res. 109, E01012. doi:10.1029/2003JE002149.
Hibbitts, C.A., Pappalardo, R.T., Hansen, G.B., McCord, T.B., 2003. Carbon dioxide on Ganymede. J. Geophys. Res. 108, 5036. doi:10.1029/2002JE001956.
Hodges, C.A., 1978. Central pit craters on Mars. Lunar Planet. Sci. IX, 521–522.
Hodges, C.A., Shew, N.B., Clow, G., 1980. Distribution of central pit craters on Mars. Lunar Planet. Sci. XI, 450–452.
Kagy, H.M., Barlow, N.G., 2008. Topography of northern hemisphere martian central pit craters. Lunar Planet. Sci. XXXIX. Abstract 1166.
Lange, M.A., Ahrens, T.J., 1983. The dynamic tensile strength of ice and ice–silicate mixtures. J. Geophys. Res. 88, 1197–1208.
Lange, M.A., Ahrens, T.J., 1987. Impact experiments in low-temperature ice. Icarus 69, 506–518.
McCord, T.B. et al., and the NIMS Team, 1998. Non-water-ice constituents in the surface material of the icy Galilean satellites from the Galileo Near-Infrared Mapping Spectrometer investigation. J. Geophys. Res. 103, 8603–8626.
McCord, T.B., Hansen, G.B., Hibbitts, C.A., 2001. Hydrated salt minerals on Ganymede's surface: Evidence of an ocean below. Science 292, 1523–1525.
McKinnon, W.B., Schenk, P.M., 1995. Estimates of comet fragment masses from impact crater chains on Callisto and Ganymede. Geophys. Res. Lett. 22, 1829–1832.
Melosh, H.J., 1989. Impact Cratering: A Geologic Process. Oxford Univ. Press, New York. 245pp.
Murchie, S.L., Head, J.W., Plescia, J.B., 1989. Crater densities and crater ages of different terrain types on Ganymede. Icarus 81, 271–297.
Neukum, G., Wagner, R., Wolf, U., Ivanov, B.A., Head, J.W., Pappalardo, R.T., Klemaszewski, J.E., Greeley, R., Belton, M.J.S., and Galileo SSI Team, 1998. Cratering chronology in the jovian system and derivation of absolute ages. Lunar Planet. Sci. XXIX. Abstract #1742.
Noll, K.S., Johnson, R.E., Lane, A.L., Domingue, D.L., Weaver, H.A., 1996. Detection of ozone on Ganymede. Science 273, 341–343.
Oberbeck, V.R., 2009. Layered ejecta craters and the early water/ice aquifer on Mars. Meteorit. Planet. Sci. 44, 43–54.
Pappalardo, R.T., Collins, G.C., Head III., J.W., Helfenstein, P., McCord, T.B., Moore, J.M., Prockter, L.M., Schenk, P.M., Spencer, J.R., 2004. Geology of Ganymede. In: Bagenal, F., Dowling, T., McKinnon, W. (Eds.), Jupiter: The Planet, Satellites, and Magnetosphere. Cambridge Univ. Press, Cambridge, pp. 363–396.
Passey, Q.R., Shoemaker, E.M., 1982. Craters and basins on Ganymede and Callisto: Morphological indicators of crustal evolution. In: Morrison, D. (Ed.), Satellites of Jupiter. Univ. of Arizona Press, Tucson, pp. 379–434.
Pierazzo, E., Artemieva, N.A., Ivanonv, B.A., 2005. Starting conditions for hydrothermal systems underneath martian craters: Hydrocode modeling. In: Kenkmann, T., Hörz, F., Deutsch, A. (Eds.), Large Meteorite Impacts III, Geol. Soc. of Am. Special Paper 384, pp. 443–457.
Pilcher, C.B., Ridgway, S.T., McCord, T.B., 1972. Galilean satellites: Identification of water frost. Science 178, 1087–1089.
Pollack, J.B., Witteborn, F.C., Erickson, E.F., Strecker, D.W., Baldwin, B.J., Bunch, T.E., 1978. Near-infrared spectra of the Galilean satellites: Observations and compositional implications. Icarus 26, 271–303.
Proctor, L.M. et al., 1998. Dark terrain on Ganymede: Geological mapping and interpretation of Galileo Regio at high resolution. Icarus 135, 317–344.
Proctor, L.M., Figueredo, P.H., Pappalardo, R.T., Head, J.W., Collins, G.C., 2000. Geology and mapping of dark terrain on Ganymede and implications for grooved terrain formation. J. Geophys. Res. 105, 22519–22540.
Schenk, P.M., 1991. Ganymede and Callisto: Complex crater formation and planetary crusts. J. Geophys. Res. 96, 15635–15664.
Schenk, P.M., 1993. Central pit and dome craters: Exposing the interiors of Ganymede and Callisto. J. Geophys. Res. 98, 7475–7498.
Schenk, P.M., 2002. Thickness constraints on the icy shells of the Galilean satellites from a comparison of crater shapes. Nature 417, 419–421.
Schenk, P.M., Chapman, C.R., Zahnle, K., Moore, J.M., 2004. Ages and interiors: The cratering record of the Galilean satellites. In: Bagenal, F., Dowling, T., McKinnon, W. (Eds.), Jupiter: The Planet, Satellites, and Magnetosphere. Cambridge Univ. Press, Cambridge, pp. 427–456.
Schultz, P.H., 1976. Moon Morphology. Univ. Texas Press, Austin. 626pp.
Senft, L.E., Stewart, S.T., 2009. The role of phase changes during impact cratering on icy satellites. Lunar Planet. Sci. XL. Abstract 2130.
Sill, G.T., Clark, R.N., 1982. Composition of the surfaces of the Galilean satellites. In: Morrison, D. (Ed.), Satellites of Jupiter. Univ. of Arizona Press, Tucson, pp. 174–212.
Smith, E.I., 1976. Comparison of the crater morphology–size relationship for Mars, Moon, and Mercury. Icarus 28, 543–550.
Smith, B.A., Briggs, G.A., Danielson, G.E., Cook II., A.F., Davies, M.E., Hunt, G.E., Masursky, H., Soderblom, L.A., Owen, T.C., Sagan, C., 1977. Voyager imaging experiment. Space Sci. Rev. 21, 103–127.
Smith, B.A. et al. 1979. The Jupiter system through the eyes of Voyager 1. Science 204, 951–972.
Spencer, J.R., Calvin, W.M., Person, M.J., 1995. CCD spectra of the Galilean satellites: Molecular oxygen on Ganymede. J. Geophys. Res. 100, 19049–19056.
Strom, R.G., Woronow, A., Gurnis, M., 1981. Crater populations on Ganymede and Callisto. J. Geophys. Res. 86, 8659–8674.
Wood, C.A., Head, J.W., Cintala, M.J., 1978. Interior morphology of fresh martian craters: The effects of target characteristics. Proc. Lunar Sci. Conf. 9, 3691–3709.
Woronow, A., 1981. Preflow stresses in martian rampart ejecta blankets: A means to estimating the water content. Icarus 45, 320–330.
Zahnle, K., Dones, L., Levison, H.F., 1998. Cratering rates on the Galilean satellites. Icarus 136, 202–222.
Zahnle, K., Schenk, P., Levison, H., Dones, L., 2003. Cratering rates in the outer Solar System. Icarus 163, 263–289.